

Article

Discovery of the Universal tRNA Binding Mode for the TsaD-like Components of the t⁶A tRNA Modification Pathway

Boguslaw Stec 

Department of Mathematics, University of Maryland General Campus, 3501 University Blvd. East, Adelphi, MD 20783, USA; bog.stec.2010@gmail.com

Abstract: Covalent addition of the threonylcarbamoyl group to N(6) of adenosine 37 (t⁶A modification) within the anticodon loop of several tRNAs is central to the translational fidelity in all known organisms. Structures for each of the enzyme components in the Tsa (t⁶A) pathway from all three kingdoms of life have been determined previously. In order to shed light on the poorly defined final step of t⁶A tRNA modification by TsaD-like components, we performed modeling studies. By docking a tRNA substrate molecule onto reanalyzed complete models of three TsaD-like proteins—TsaD from *T. maritima*, Qri7 from bacteria, and Kae1 from yeast—we identified a binding site that is common to all of them. An apparently universal binding mode has perfectly oriented tRNA for catalysis by TsaD. Furthermore, it suggests how the conformational changes in TsaD, in response to the binding of the additional regulatory subunits, control enzymatic activity. Re-refinement of the X-ray structure of the TsaBDE complex from *T. maritima* tentatively suggests that the moiety bound at the active site of the TsaD component is threonylcarbamoyl-AMP (TC-AMP). These findings suggest a detailed model for the mechanism of the catalytic reaction carried out by the TsaD-like components that explains the transfer of unstable TC-AMP from TsaC to TsaD proteins in the t⁶A modification pathway.

Keywords: ATPase; modified nucleoside; transfer RNA; tRNA; essential enzymes



Citation: Stec, B. Discovery of the Universal tRNA Binding Mode for the TsaD-like Components of the t⁶A tRNA Modification Pathway.

Biophysica **2023**, *3*, 288–306. <https://doi.org/10.3390/biophysica3020019>

Academic Editors: Ricardo L. Mancera, Paul C Whitford and Chandra Kothapalli

Received: 16 February 2023

Revised: 6 April 2023

Accepted: 7 April 2023

Published: 12 April 2023



Copyright: © 2023 by the author. Licensee MDPI, Basel, Switzerland. This article is an open access article distributed under the terms and conditions of the Creative Commons Attribution (CC BY) license (<https://creativecommons.org/licenses/by/4.0/>).

1. Introduction

The biosynthesis of N(6)-threonylcarbamoyladenosine (t⁶A) appears to be a universal tRNA modification present in all three kingdoms of life. Different sets of proteins function in eukaryotes and bacteria to produce this modification. Many of the components show significant homology and common biochemical reactivity. In bacteria, the t⁶A modification pathway is a complex multistep process that involves a family of proteins: TsaB, TsaC/TsaC2, TsaD, and TsaE [1–5]. It is well demonstrated that the TsaC/C2 protein (threonylcarbamoyl-AMP synthase) catalyzes the condensation of Thr-CO₂/CO₃-ATP to obtain an unstable intermediate, threonylcarbamoyl-AMP (TC-AMP) [6].

It is commonly accepted that the direct interaction of TsaC/C2 with the TsaD component is responsible for the channeling and direct transfer of this intermediate into the active site of the TsaD, where the final step of the pathway is catalyzed. This theory was derived from arguments from genomic analysis [7], but they have not been demonstrated experimentally. This belief is also based on the observation that under normal conditions there is an insufficient concentration of the freely available, unstable intermediate TC-AMP (half-life time ~3.5 min) [6]. Such a shortage of the unstable intermediate would be even more pronounced under conditions of induced stress, which usually stimulates rapid tRNA synthesis [8]. Additionally, such a view is reinforced by the existence of the structurally homologous bifunctional enzymes TobZ [9] and HypF [10], which have dual functionality corresponding to a fused pair of TsaC/TsaD. At the final step, the TsaD is primed by forming a complex with tRNA to transfer the threonylcarbamoyl (TC) moiety from the AMP group of TC-AMP onto the N6 of adenosine 37 of the incoming tRNA molecule [1,2,4], thus completing the synthesis of this important tRNA modification.

Several other important interactions were experimentally demonstrated, such as the fact that in many bacteria there exists a stable complex of TsaBD [4]. Additionally, the direct competition of tRNA with the TsaE component for binding to the TsaBD complex was also demonstrated [4,11]. It was surprising that the binding of TsaE also stimulated the tRNA binding [4], below the concentration range necessary for competition to play a role. This fact clearly suggested that the dimer of DBBD, determined to be a basic structural unit for the complex in *T. maritima* [4], must work in an anti-cooperative manner by the binding of TsaE and tRNA molecules in opposing sites at the same time. The data suggests that the competitive binding of TsaE that forces a release of tRNA from the first site is at the same time promoting binding of the tRNA at the second site [11]. The modeling clearly suggests that TsaE must work in an antagonistic mode to both tRNA and TsaC binding. A comparison of the TsaBD complexes in the presence and absence of the E component suggests that binding of TsaE promotes the conformational change in TsaD that makes binding of tRNA easier but more difficult for binding of TsaC/C2 [4,11]. However, more experimental evidence is needed to demonstrate the direct interaction between the TsaC/C2 and TsaD components that must occur for a successful completion of the (t⁶A) modification.

Eukaryotic systems employ catalytic core proteins such as TsaC/C2 and Kae1, an analog to TsaD [7,12], but use a variety of additional proteins as regulators of the complex (Gon7/Pcc/Bud32/Cgi21) [5,12,13]. High structural and sequence homology of the central proteins, such as TsaD/Kae1/Qri7 [14], suggests a similar catalytic mechanism and a similar mode of tRNA binding while interacting with different regulatory proteins. Therefore, finding out a precise position for the bound substrate (tRNA) would offer a significant advantage in an attempt to model the active tertiary complex TsaD-(TC-AMP)-tRNA. An initial tentative model of the docked TC-AMP was published by Missouri et al. [2]. To further advance the knowledge of the details of the catalytic transfer of the TC to N6 of adenosine and shed light on the composition of this complex, we performed a modeling study in which we docked a tRNA molecule to known representatives of the TsaD-like molecules (TsaD from *T. maritima*, Qri7, and Kae1 from *S. cerevisiae*).

In order to investigate the problem of tRNA binding to the Tsa complexes in the final step of the pathway, we have retrieved all the relevant structures deposited in the PDB. We reviewed the structures of TsaC, TsaB, and TsaD, as well as TsaE and associated proteins from bacteria and eukaryotes. To obtain truly predictive results for our modeling study and for docking in particular, we needed to obtain as complete a model as possible. Special attention was paid to the recently published structure of the TsaBDE from *T. maritima* [2], elucidated by the van Tilbeurgh group, as it showed differences from a similar complex that was reported by Luthra et al. [11].

Similarly, we reviewed the structures of Qri7 and Kae1. Only marginal changes were introduced, which were needed for the completion of the model. Missing elements were crucial for the docking of tRNA. The completed structures, in combination with previous biochemical results, shed light on the role of the TsaE component in regulation of tRNA binding to the TsaD and the functioning of the TsaBD dimer. The review of the remaining molecules resulted in formulating the proposals for the catalytic mechanisms of the TsaC- and TsaD-like elements and the mode of transfer of the unstable TC-AMP intermediate from the TsaC to the TsaD.

The complete structures had a clear preference for particular docking modes of the tRNA molecule and helped establish the consensus mode for the tRNA binding pose. As a result, we proposed a tentative model of the tRNA binding to the TsaD that offers a transferability of consensus interaction across different kingdoms, species, and organelles, as well as the universality of a catalytic mechanism of action carried out by the TsaD, TsaC elements, and their analogs [14].

2. Materials and Methods

2.1. Crystallography

The protein coordinates and diffraction data for TsaBDE complex (6FPE) [2] had been extracted from PDB and imported to CCP4 to initiate the refinement to complete the structure. The mtz file was created using the F2mtz (import) option with a new test set containing 5% of data. This mtz file, together with the PDB file, was used for the refinement in Refmac [15], which was included in CCP4 release 7.0. A comparison of the refinement statistics between the initial and final models is presented in Supplementary Table S1. A similar protocol was applied to the model of Qri7 (3WUH) [16] to complete and clarify the structural details of the missing fragments as mentioned above.

2.2. Modeling

The refined models of the Qri7 dimer [16], the (TsaBDE)₂ complex [2], and a partially assembled model of the KEOPS complex containing Pcc1 and Kae1 were used in constrained docking experiments to address possible tRNA binding modes. The assembled model of the KEOPS complex containing Gon7, Pcc1, Kae1, Bud32, and Cgi121 [17] was used for further modeling and visualization. The tRNA model used for docking was taken from the crystal structure of tRNA in complex with a charging synthase (1QF6) [18]. This model explains the functional role of the chemical modification at A₃₇ and the partial unfolding of the anticodon loop. In our modeling effort, we retrieved a family of structures describing the details of the Kae1 complex [17], which were used with only small changes (PDB structures 3ENH, 3EN9, 4WW5, 4WXA) [5,12,13,17].

We also retrieved and inspected the structures describing the TsaC/C2 and TsaD analogs from different species. These were investigated in order to understand the intrinsic limitations imposed on possible catalytic mechanisms of the biosynthetic formation of the unstable intermediate TC-AMP and its transfer to the TsaD. As a result, plausible models of catalytic reactions were proposed for both components of the t⁶A cycle, TsaC/C2 and TsaD. Moreover, we were able to gain insight into the transfer mechanism of unstable TC-AMP from TsaC to TsaD by utilizing the molecular homology of this transient complex with the enzymes TobZ and HypF [9,10]. Models used for the investigation of the TsaC mechanism were 6F8Y, 6F89, 6F87, 2EQA, 3AJE, and 1HRU [19–22], while models used for TsaD modeling were 6N9A, 6S84, 6NAK, 6Z81, 4YDU, 4WQ5, 4WQ4, 3ZET, 3EN9 and 2VWB [2,11,17,23–26].

All retrieved structures were inspected for quality and completeness of the models as described above. The structures used in modeling were thoroughly checked against their X-ray data. The completed PDB structures of the TsaBDE complex and Qri7 provided a proper description of conformational mobility. The test for mobility and segmental motions was performed by using TLSMD web service [27], which uses the distributions of the individual temperature factors in the final models. We noticed before that this method is one of the most sensitive for spotting modeling errors in macromolecular structures [28].

More detailed descriptions of the process of structural improvements to the TsaBDE complex [2] and Qri7 [16] were described in the Supplement and in [29]. Improvements in the Kae1 complex [17] (3ENH, 3EN9) provided an improved electrostatic image of the protein complex. The figures were prepared in PYMOL [30].

2.3. Docking

Docking was carried out with multiple programs (Haddock, Autodock, and NP-Dock) [31–33]. There was a limited consensus that was further explored. Haddock [31] and Autodock [32] lead to very similar results without making clear distinctions between the clusters. NP-Dock [33] produced a more focused and distinct cluster that overlapped with rather diffuse clusters of other programs; therefore, we focus on and discuss the NP-Dock results here. In order to perform docking experiments, we used the tRNA model (1QF6) [18] and all relevant protein models prepared according to the above procedures. In all docking experiments, the default program settings were used without modification.

In order to eliminate spurious solutions, we applied a constraint that placed N6 of A₃₇ of the tRNA model within a 5 Å distance to the amide bond of TC-AMP, as found in the refined model of Tsa-BDE [2], at the active site of a TsaD protein. In the initial step, 20,000 decoys were docked, individual poses were scored, and the top 100 representatives were clustered. The resulting clusters were ranked by pseudo-energy and visually inspected. For all samples, only a handful of clusters were identified for our purpose, despite the program's limitation allowing for the identification of up to 30 clusters. The clusters with the best scores were selected for analysis. The selection criteria also included that there be no significant interpenetrations/overlaps with the positions of the binding partners TsaC/C2 or TsaE, whether the interactions were predicted or experimentally determined.

3. Results and Discussion

3.1. Refinement of the TsaBDE Complex from *T. maritima* and Qri7 from Yeast

To obtain reliable results for our docking studies, aimed at elucidating the tRNA binding mode, we needed to utilize the best models for the structures of the TsaD-like elements. Only complete and well-refined structures can provide the basis for drawing conclusions based on docking. Therefore, we initiated the review of quality and the refinement of selected structures.

The coordinates and the associated diffraction data of *T. maritima* TsaBDE proteins in the 2:2:2 complex and Qri7 from yeast were retrieved from PDB (6FPE, 3WUH) [2,16]. The refinements have been completed in several macrocycles, consisting of a round of visual inspection and manual modeling/correcting of the structures, followed by ~20 cycles of LSQ refinement in Refmac 5.8. The structures were improved by modeling the difference in electron densities, by placing or removing protein fragments, and by repositioning other fragments. This procedure led to improvements in the overall completeness of the model. The main descriptors like R and R_{free} improved, while the resulting model maintained good stereochemistry despite modeling fragments with weaker electron densities at lower contouring levels.

The refined structure showed improvements to the initial model in the backbone placement (Figure S1) as well as many side-chains as measured by comparison to other models, particularly [11]. The final model of the refined TsaBDE complex (6NAK) contains more than 50 newly placed residues and more than 190 residues in new positions. This constitutes more than 15% of the full sequence of the original structure. The newly refined elements improved the standard R factor (0.19 from the original 0.22) while leaving the R_{free} at the same level. The detailed findings are described in the Supplement.

All the improvements lead to two new elements that deserve mentioning as they contribute to a better understanding of the function of this complex. The electron densities suggested the presence of a substrate, TC-AMP (Figure 1), in both active sites of TsaD subunits instead of the originally placed PEG and glycerol. Additionally, binding of the TsaE component caused a significant reorganization of the 40–50 loop in both TsaD subunits (Figure 2) that was not modeled in the original determination. This conformational transition in TsaD, caused by the binding of TsaE, must be associated with the alternative/antagonistic binding of tRNA or TsaC to the active site, as described in [11]. The TsaE element therefore plays a controlling and releasing function in opposition to the suggested role of causing disorder at the active site [2]. The refined TC-AMP at the active site sheds light on the catalysis by the TsaD component of the t6A pathway and the transfer paths of unstable product/substrate TC-AMP from the TsaC/C2 to TsaD.

Including the substrate TC-AMP in the model improved the electron density at the active site and suggested the presence of partially occupied metal ions. Zinc ions were refined with 40% occupancy at both active sites, which was fully compatible with partially disordered binding residues, which were identified before in [11] (His109, His113, His137, Asp296). Its coordination sphere is looser than that in 6N9A, with longer bonds to the ligands and His137 not interacting with the Zn ion. Binding of the substrate apparently caused disordering of the region 291–294 as indicated by weaker electron density. These

changes resulted in a transition to a more twisted/open conformation of the TsaD that is visualized in Figure 2. The substrate binding domain shows a noticeable displacement and rotation of 17° as compared to the reference structure of the *E. coli* TsaB-TsaD heterodimer (4YDU) [24]. The observed opening of the active site cavity (Figure 2B) must have functional significance, as binding of the tRNA to the active site cleft would require the breathing motion to bring the A37 close to the reactive center located at the TC-AMP molecule.

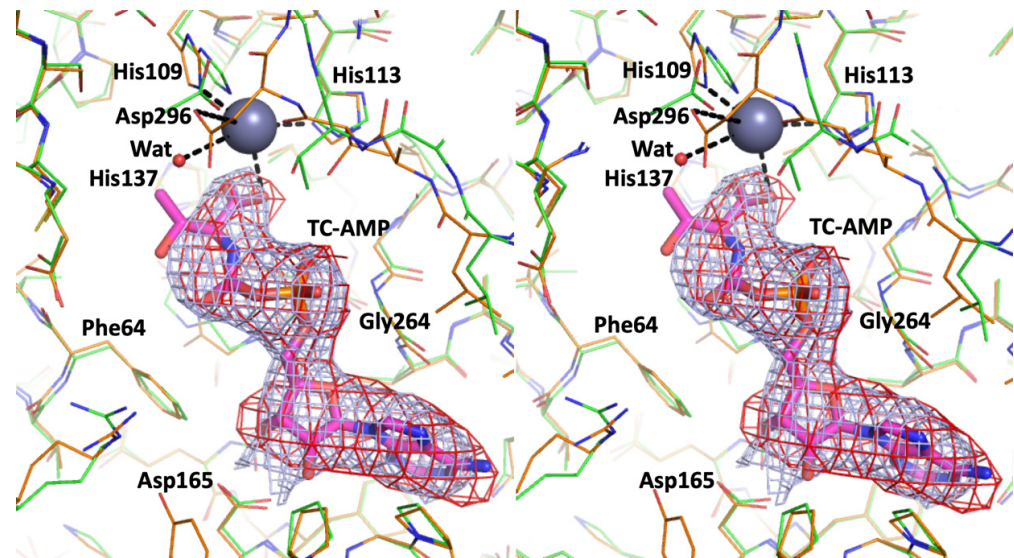


Figure 1. The stereo representation of the final model with the TC-AMP molecule in the active site of the TsaD component (6NAK) covered with electron density maps. The omit map is in red (3σ) phased with the original model (6FPE), and the 2Fo-Fc ED map is contoured at a 1.3σ level in bluish-gray phased with the final refined (6NAK) model. The final refined model (6NAK) is in orange, while the initial model (6FPE) is in green. The large gray sphere represents the zinc atom refined with 40% occupancy.

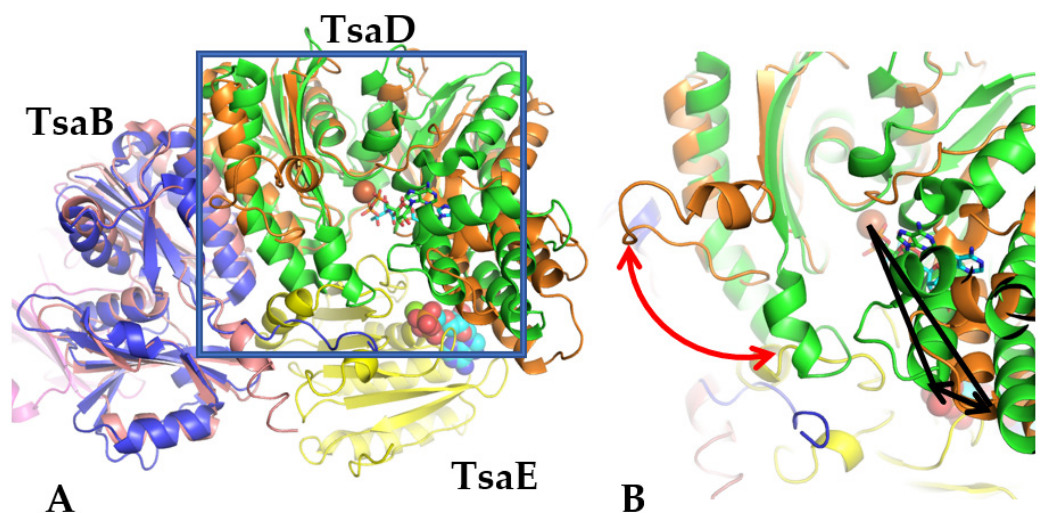


Figure 2. Superposition of the models of TsaBD dimers (YgjD–YeaZ) from *E. coli* (4YDU) and the refined model of TsaDBBD dimers from *T. maritima* with the TsaE bound (6NAK). (A) The comparison of the BD dimer conformations: blue and green are *E. coli* BD subunits, pink and orange are *T. maritima* BD subunits, and the E subunit is in yellow. (B) A close-up of the model presented in (A), enclosed by the box, shows the conformational change of the 30–50 region in TsaD, denoted by a red arrow, caused by binding of TsaE. The breathing movement between the domains is indicated by a black arrow upon direct superposition of the N-terminal domain of TsaD.

The comparison of the *E. coli* TsaBD complex with the *T. maritima* TsaBDE complex clearly suggests that the binding of TsaE creates a conformational change that would prevent the TsaC binding or, alternatively, its expulsion from the dimeric TsaCD complex, while at the same time it opens up the TsaD active site cleft, thus promoting the tRNA binding upon dissociation from the complex. The new model of the TsaBDE complex achieves consensus with the newer model described in [11] as well as with the corrections introduced to the recently published model [2]. An important consequence of the new model was an altered electrostatic signature that allowed for successful docking of the tRNA. The tentative localization by X-ray crystallography of the TC-AMP also contributed to the success of this procedure by providing a key constraint for the tRNA docking. Our success in identifying the TC-AMP at the active site is clearly confirmed by the capture of the stable substrate analog in the TsaBD complex from *E. coli* [23].

The Qri7 structure was refined well, with small changes to the original model that were contained to the mobile loops 70–80 that are analogous to the loops 40–50 in TsaD. The modeling of the missing elements proved to be important in understanding the tRNA binding. The final model showed again a modest improvement in both R and Rfree for a complete model. An important change was proposed: the repacking of both subunits so they were organized in the dimer with biological relevance. Only this new dimeric form was used in subsequent docking experiments. The packing of the interface in the D-D dimer of Qri7 (6NBJ) formed a four-helical bundle reminiscent of the B-D interface in the *T. maritima* complex (6NAK, 6N9A) [11].

The models representing different complexes of the yeast KEOPS system were visually inspected, but as a result, they were only marginally changed and are not described in detail. However, appropriately superposed subunits were used to understand the conformational transitions facilitating the binding of multiple elements, such as auxiliary proteins and tRNA, and the transfer of substrates between subunits interacting during the cycle. These comparisons were also used for proposing and understanding the catalytic cycles for TsaC/C2 and TsaD and understanding the roles of individual domains in Sua5 as well as the mobility of domains in TsaD. Finally, they were indispensable in proposing the catalytic mechanisms for converting TsaC to TsaD and the transfer pathway for catalytic intermediates between TsaC and TsaD active sites, as described below.

3.2. Main Structural Changes to the DBBD Dimer Caused by Binding of the TsaE Element as Compared to Structural Changes in Qri7 and KEOPS Complex

The existing models for all components (TsaC/B/D/E) were mutually compared to the previously solved and deposited models, such as, for instance, 3ZEU [25] for the TsaBD complex, 2A6A [33] for the YeaZ dimer of TsaB [34], or 1HTW for TsaE [35]. During Qri7 modeling, both deposited models were used for comparisons (3WUH, 4K25) [16,36].

Recent findings shed light on the role of TsaE in controlling the activity of BD or DBBD complexes [11]. Binding of TsaE competes with tRNA, but at the same time it primes the TsaBD complex for binding to tRNA [4]. Luthra et al. [4,11] demonstrated that this general control is exerted by the ATPase activity of the E component. In Qri7 [36], the TsaD-like element forms a TsaD homodimer by forming the four-helical bundle at the interface. Therefore, the absence of other protein components needed in other complexes for activating the dimer means that only the internal mobility of the protein controls tRNA binding. The Qri7 dimer appears to be the simplest and most basic complex to study the tRNA-TsaD interaction, therefore it should have the most distinct signature/motif for binding.

The bacterial TsaBD interface is highly similar to the interface in Qri7 (D-D homodimer), with a four-helical bundle formed by the helices from B and D components. The TsaBD heterodimer in *T. maritima* followed the same logic at the BD interface but allowed for additional control by conformational changes in the TsaB element, particularly in the C-terminal helix, as seen in the comparison of 6N9A and 3ZEU [11,25]. This heterodimeric architecture creates an additional possibility for control of the complex through the binding

of an additional element, TsaE. The control is accomplished by a significant conformational change in the region 30–50 of TsaD upon TsaE binding. The model of this fragment with the corresponding electron density is shown in Figure S3. For instance, in the *T. maritima* TsaBDE complex, upon binding of subunit E, there is an almost 90 degree rotation of this fragment away from subunit D, which is coupled with an opening of the active site cleft (around 17°) located at the junction of two domains of the D subunit (Figure 2). Additionally, this change is accentuated by a transition from an extended to a helical conformation in the C-terminal fragment of TsaB. This complicated conformational transition is clearly illustrated by superposing the TsaBD heterodimer from *E. coli* (4YDU) [2] onto that in the *T. maritima* TsaBD complex (Figure 2).

The *E. coli* and *B. subtilis* complexes can be understood as half-complexes of *T. maritima*. The *E. coli* structure shows a much narrower cleft, at the apex of which the active site is located. Presumably, control of opening of this cleft is also needed for the binding of tRNA and transfer of the TC group to A37. As depicted in Figure 2, the TsaE subunit clearly penetrates and clashes with the 30–40 fragment of the TsaD subunit in the *E. coli* model, which results in the conformational transition mentioned above.

A similar change is observed in several KEOPS complexes. Binding of the Bud32 causes a significant rotation of the C-terminal helix, which protrudes into the space occupied by the postulated binding of tRNA. Therefore, the ATPase activity of Bud32 would exert a similar effect on the KEOPS complex in eukaryotes as the ATPase activity of TsaE in the BDE complex in bacteria [11], despite a different fold and different location in the complex [17].

3.3. Modeling of the tRNA Binding to the TsaD-like Subunits of the t^6A_{37} Eukaryotic and Prokaryotic Complexes

The placement of TC-AMP at the active site of the TsaD component defined a specific location for the approaching A37 of the anticodon loop of tRNA (Figures 3B and 4A). For the effective transfer of the threonylcarbamoyl group of TC-AMP to N6 of A37 to occur, the most likely position for N6 of the adenosine should be located within a 3.5 Å sphere around the TC-AMP scissile bond. Applying this constraint, we performed a comprehensive docking experiment utilizing all three representative complexes from mitochondria (Qri7), yeast (KEOPS), and *T. maritima* (TsaBD 2:2 dimer) known to produce t^6A_{37} .

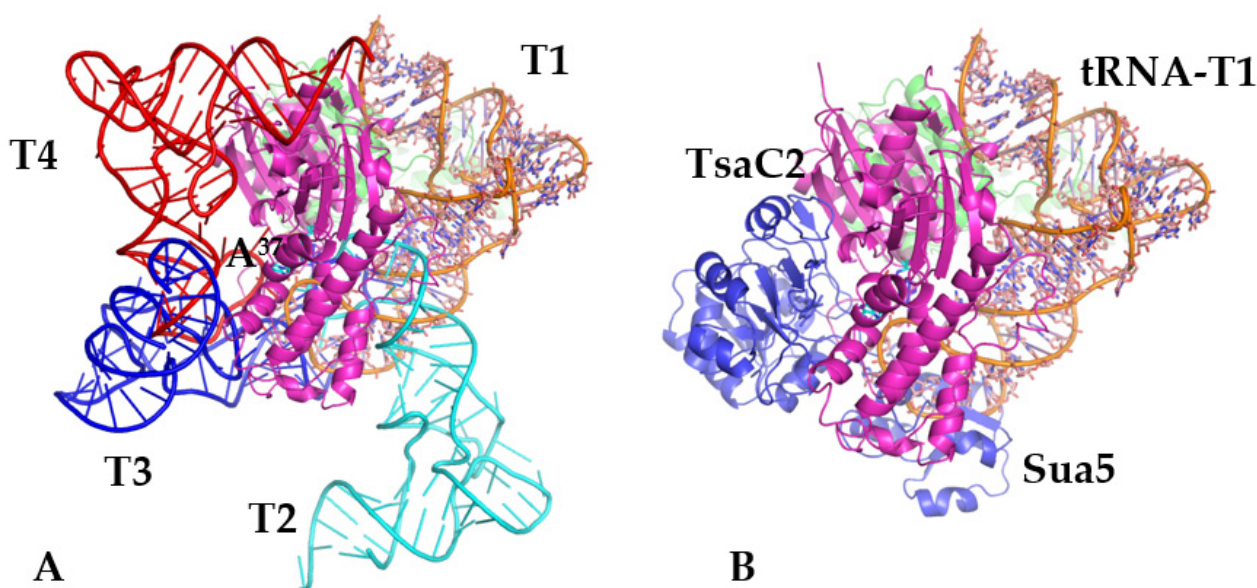


Figure 3. The docking of the tRNA to the TsaD subunit (and homologs). Docking was performed with a constraint between a protein and the A37 of the tRNA molecule. A sphere drawn next to the

TC-AMP represents the site of constraint. Both panels are in the same side-view orientation. (A) The four poses, representing dominant solutions fulfilling the constraint, are shown in orange, light blue, dark blue, and red. The best pose (T1) is in orange. The pose T3 coincides with that described in [11]. (B) The TsaD-like subunit (in magenta) with the tRNA docked (in orange) representing cluster T1 is presented on the right-hand side. On the left-hand side of the TsaD subunit, there is TsaC2 (in blue), modeled as suggested by the domain disposition in TobZ. This TsaC placement represents a transient binding complex capable of synthesizing the unstable TC-AMP on site and transferring it to TsaD. The Sua5 domain is loosely attached in an open conformation, as suggested by the small-angle scattering results.

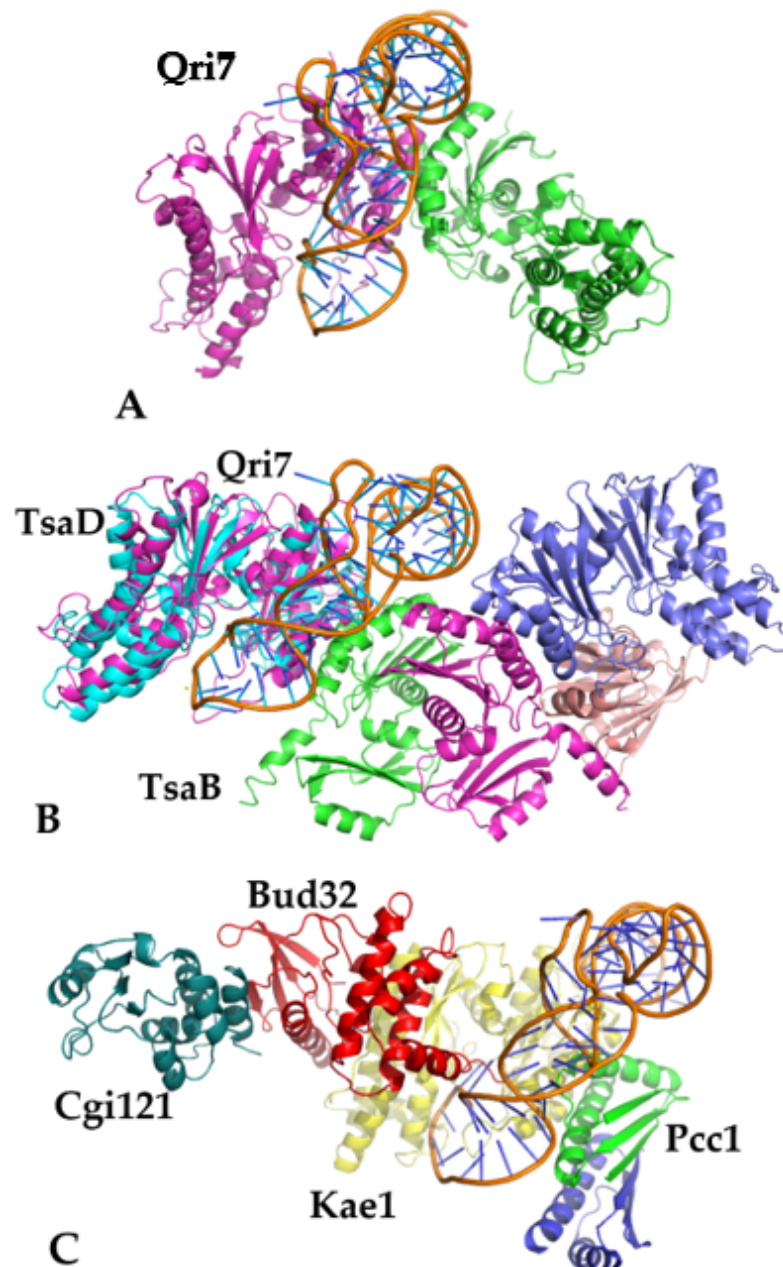


Figure 4. The view of the TsaD proteins from different sources, with predicted consensus poses of tRNA docked to the eukaryotic and prokaryotic complexes of t6A synthesis that all correspond to pose T1 in Figure 3. (A) Qri7 homodimer with the docked tRNA. (B) *T. maritima* B₂D₂E₁ + tRNA (TsaD in light blue is superposed on the Qri7 monomer from (A) in purple). (C) Kae1 complex from yeast with tRNA. The Kae1 subunit, which is a homolog of TsaD, is in yellow.

The docking experiments were carried out using the tRNA molecule from (1QF6) [18], which was docked to the refined version of the complete Qri7 dimer, the DBBD dimer of the *T. maritima* complex described in this report (with TsaE omitted), and the partially reconstituted model of the yeast KEOPS complex of Kae1 with Pcc1. The full model of the yeast KEOPS complex with Kae1, Pcc1, Bud32, and Cgi121 was later used for visualization purposes and is shown in Figure 4. The web service NPDock [33] was used for docking experiments with the tRNA model that was extracted from PDB. The default settings of the program were used without post-refinement. The program produced 20,000 decoys/poses that were scored. Subsequently, the program clustered the 100 top solutions into 30 clusters. Only around 10 significantly populated clusters were identified within the limit of the 5 Å RMSD. The top four representative poses/clusters are shown in Figure 3. All these poses, shown in Figure 3A, allow for the N6 of A₃₇ to be positioned near the TC moiety and provide marginal but sufficient binding energy with the protein. Subsequently, more detailed criteria described below were applied, which indicated that cluster T1 was the most likely.

For selecting the best pose among the four dominant solutions (T1–4), the following rules were adopted: (1) the highest position on the pseudo-energy ranked list; (2) the best geometrical arrangement of A₃₇ for the transfer of the TC moiety; and (3) the pose should have minimal interpenetration with volumes of auxiliary binding proteins (especially TsaC/C2 or TsaE) necessary for production and translocation of TC-AMP. Out of the four best clusters (T1–T4), only one satisfied all the conditions, which was T1. This pose has the most extensive protein-RNA contacts; it partially contacts the second molecule across the dimer interface, excluding the second molecule's binding, and shows optimal capability for access to the active site of TsaD as the extended anticodon loop of the tRNA can easily be inserted into the active site (Figure 3B). This approach would result in minimal distortion of the tRNA, similar to the one reported in 1QF6.

Out of three protein targets, the best score in pseudo-energy was obtained for Qri7, which lined up well with the expectation that Qri7 should be the best and minimal model for this interaction. The *T. maritima* DBBD model produced intermediate results, while the least distinct solution was obtained for the Kae1 complex, as expected since this complex is the most regulated and serves multiple purposes. However, the best solution/poses for each protein-tRNA complex were in general agreement with each other, thus establishing a consensus binding pose that is utilized by the entire family, regardless of the presence of the auxiliary proteins (Figure 4). This observation suggests a possible pathway for increasing regulatory control by the gradual addition of individual proteins to the catalytic core built around the TsaD subunit. This conclusion is supported by recent observations that the TsaE component in the TsaBDE complex [4,24], as well as Bud32 in the KEOPS complex [5], bind independently and control tRNA binding by ATP hydrolysis at the site located at the interface between TsaD and TsaE or Bud32.

The universality of the binding pose for tRNA proposed in this report raises a very interesting question. Why are so many vastly different complexes involved in the same catalytic role of transferring the TC group to the A₃₇. The manner of tRNA binding described above can be regulated by the binding of auxiliary proteins. Alternative functions performed by these complexes provide an attractive hypothesis for explaining why such a variety of complexes exist. The eukaryotic KEOPS complex is known to possess DNA binding capabilities as well as telomere editing activity [37]. This activity may require an increased ability to bind longer stretches of DNA, and such binding would be difficult to accomplish with a single Qri7-like dimer [36]. The binding of auxiliary proteins not only provides control over the activity of the complex but apparently also increases binding. Therefore, the changes in composition of complexes contribute to the modulation of additional functions. New results show that the dimerization of the Kae1 complex through Pcc1 is not necessary for tRNA activity [5], while this dimerization event may be required for DNA telomerase activity [37].

Recently, two teams reported models of tRNA bound to complexes containing TsaD [11,38] derived from small-angle scattering experiments. These tentative models were constructed by fitting the tRNA molecules into the reported excess density extending from the fitted protein elements. In both cases, the incoming tRNA was interpreted as lying along the main axis of the complex. In TsaBD from *T. maritima* [11], the tRNA was fitted into the experimental density along the body of TsaD. A similar arrangement was detected in the full KEOPS complex, reinforced by the interpretation that the acetyl terminus of tRNA binds to Cgi121 [38]. Guided by this observation, the authors of [38] proposed that this pose represents the catalytically active complex of the tRNA with TsaD and extended this observation to all known TsaD representatives. The modeled complexes are presented in Supplementary Figure S4h,i of [38]. This model was reiterated by Beenstock & Schicheri [39] in an excellent review paper that summarized the KEOPS results, as well as in the latest review [1]. The pose proposed for KEOPS was applied to other TsaD representatives, despite the fact that in Qri7 and other TsaBD complexes, the interface would be smaller and apparently insufficient to form a stable complex. The same paper stated that Cgi121 is expressed in sub-stoichiometric ratios to the remaining components of the complex, thus undermining the conclusion that Cgi121 participates in the catalytically active tRNA complex. Additionally, van Tilbeurgh [13], through studying the association of Bud32 with Cgi121, concluded that Cgi121 cannot participate in the active complex as its deletion does not inhibit the synthesis of t⁶A modification [12,39,40].

In both complexes, this conformation of the tRNA would make the approach to the active site very difficult with the anticodon loop at the productive conformation, as suggested by [6]. Additionally, this pose would interfere with the regulatory roles of TsaE or Bud32. Therefore, one can conclude that both experimental results, which are based on small-angle scattering, can be interpreted as a transient binding that is detected in its early stages and that conforms to one of the four solutions described above for the tRNA bound to the TsaD (pose T3). Particularly, binding of tRNA to Cgi121 should be treated as an initial contact phenomenon in which Cgi121 fulfills the role of the tRNA chaperone to bring it up close to the large KEOPS complex. However, it is less mobile than its bacterial counterparts to effectively perform the assigned function. These arguments are reinforced by noticing that the KEOPS complex performs the catalysis with the telomeres as a substrate, which are larger in size than a single tRNA molecule.

3.4. Modeling of the Catalytic Reaction of TsaD

To facilitate the formulation of the proposal for the catalytic reaction carried out by the TsaD, we utilized the 3-D model of the substrates bound to its active site. The refinement suggested a location of the TC-AMP (6NAK) that was confirmed later by the structure 6Z81, as well as the placement of the A37 by docking of the tRNA. The corrected and refined model of a BDE dimer (6NAK, derived from 6FPE) was used for docking of tRNA with the threonylcarbamoyl modification (TC) removed (1QF6). Before docking, the E element was removed from the model, and in one of the D subunits, the region 30–50 was modeled in a conformation corresponding to the structure of the BD dimer from bacteria (4YDU) that attains a more extended conformation. The manually adjusted pose/decoy number 13,497 was used as the representative of the tRNA binding mode to the TsaD. Such a model was used for modeling the catalytic reaction and is presented in Figure 5 and Figure S6.

The location and orientation of the TC-AMP in the active site of the TsaD component allow for formulating a proposal for the catalytic mechanism carried out by TsaD. Such a mechanism is further supported by the structural results of the TC-AMP analog bound to the *E. coli* TsaBD complex (6Z81) [23]. The mechanism of transfer of the threonylcarbamoyl moiety can be postulated as a nucleophilic attack of the activated N6 nitrogen of adenosine on the bridging carbamate group of TC-AMP, followed by the formation of an unstable tetrahedral intermediate (Figure 5A,B). This spatial arrangement takes advantage of a partial resonant structure of the carbamate, reminiscent of a peptide amide bond in peptides, that allows for the proteolytic activities of different agents/nucleophiles in several classes of

proteases. The unstable tetrahedral intermediate would later collapse to the final product, driven by AMP as a leaving group. Therefore, the location of the flat face of the carbamate group in TC-AMP defines the location of the approaching N6 of the adenosine at the side directionality with sufficient accuracy for modeling (Figures 3B and 5A). The position for a deprotonated N6 is defined by the face-to-face contact of the adenosine ring at position 37 and the amide bond plane of TC-AMP, which is bracketed on the opposite site by a loop containing Cys10 in *T. maritima*.

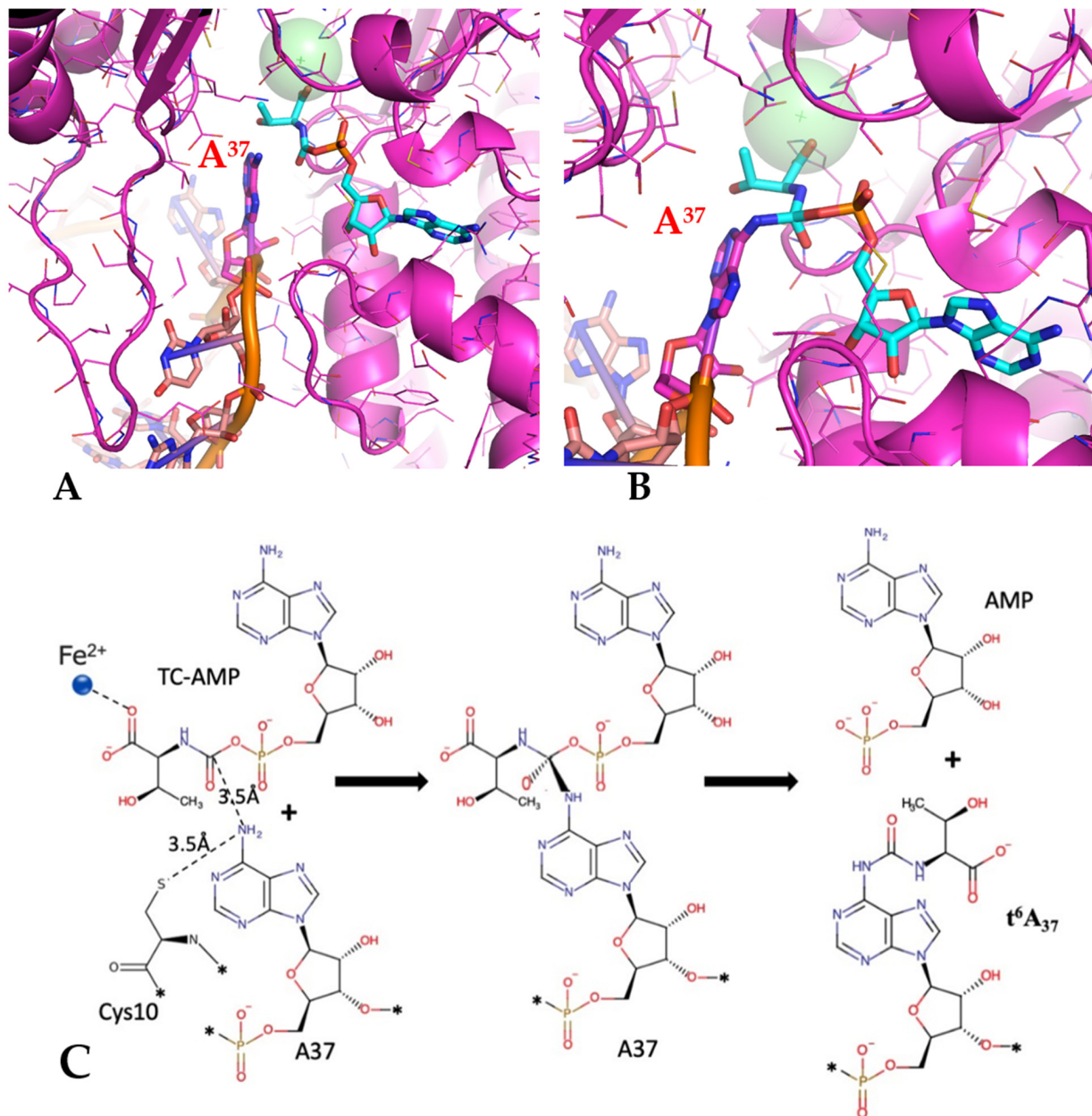


Figure 5. (A) A close-up of the active site of the Tsad-like subunit (Qri7) with the tRNA docked as in Figure 3B, in a competent position to directly interact with the TC-AMP bound to the Zn metal ion (in light green). The anticodon loop of the tRNA is buttressed by two mobile loops of Qri7. Adenosine 37 of the bound tRNA interacts directly with TC-AMP. N6 approaches closely to the carbonyl, while N3 is in the vicinity of the Thr O_y moiety to allow for hydrogen bond formation. (B) The schematic of the unstable tetrahedral intermediate formed by the nucleophilic attack of the deprotonated N6 of A37 on the carbonyl of TC-AMP. The unstable intermediate collapses to form TC-modified tRNA and AMP. (C) The schematics of the reaction catalyzed by Tsad. Upon binding of the tRNA with a

partially unfurled anticodon loop that inserts itself into the active site, the closeness of Cys10 stabilizes the deprotonated form of N6 adenosine 37. The breathing motion of the active site cavity of TsaD promotes a close approach of the N6 to the flat face of the TC-AMP amide bond. This approach, in concert with the polarization imposed by close contact with the metal ion, leads to the formation of the unstable tetrahedral intermediate around the carbon atom. The subsequent collapse of the intermediate leads to the transfer of L-threonine through the formation of an amide bond to the adenosine 37 with simultaneous release of AMP. * stands for an arbitrary bonding atom, i.e., there is a remaining part.

The only remaining issue, besides a precise location of the adenosine ring determined by the tRNA directional approach, which is controlled by the three-dimensional organization of the active site cleft in TsaD, is the mechanism of activation/deprotonation at N6 of A37. As is well remembered from the early days of DNA modeling, the main contribution to the discovery of DNA structure by Watson and Crick was the fact that the bases can be present in solution in different tautomeric states [41,42]. Therefore, full and controlled deprotonation of adenosine at N6 is not needed for the reaction to proceed. Complete deprotonation is heavily disadvantaged by a high pKa value of N6. Instead, an internal proton migration between N6 and N1 to form a different tautomeric state would be preferred. Therefore, only a partial stabilization of one of the presented states is needed for the reaction to proceed without an elaborate deprotonation mechanism required by acid-base reactions. The best candidate for such stabilization in *T. maritima* is a member of the highly conserved sequence SCDE, i.e., Cys10 of TsaD, which in the crystal structure (6NAK) is located with its S γ group around 7 Å away from the flat face of the scissile bond in TC-AMP, therefore in close proximity to the inserting N6. The size of the active site cleft is perfectly suitable for insertion of the individual base, and it is compatible with helical separation of bases in nucleic acids, therefore providing direct van der Waals contacts. The protonation state of Cysteine residue is most likely controlled by the closeness of the charged residues at the loop (SCDE) and an additional contact with Asp296 that participates directly in the binding of the metal ion at the active site of TsaD. The model of the transition state of the proposed reaction is presented in Figure 5B, and the postulated reaction's schematic is presented in Figure 5C.

Figure 3B shows the model of a ternary binding complex of TsaC2 (threonylcarbamoyl synthase) and tRNA to TsaD. This model shows a tentative location of the Sua5 domain, which is highly mobile, as was suggested by small-angle scattering studies of the mobility of TsaC2 from *B. burgdorferi* [43]. Even though the model places tRNA and TsaC on opposite sides of the TsaD subunit of the complex, their binding must be transient and anti-cooperative, as all experimental attempts to capture these complexes have so far been unsuccessful. Additionally, binding of TsaE must be antagonistic to binding of both tRNA and TsaC, as suggested by experimental results [10] and inferred from overlap of different components when these are modeled bound to TsaD simultaneously.

3.5. Modeling of the Catalytic Reaction of TsaC

The mutual orientation of the TsaC versus the TsaD can be well modeled (Figure 3) in analogy to the domain organization of the structure of TobZ. This model suggests a clear path of transfer for unstable TC-AMP between both active sites that are separated by around 15 Å in TobZ as well as in our model. It is well documented that unstable intermediates are protected at the active sites of enzymes in internal protein cavities [44,45] and can survive for much longer times than their natural half-lifetime in solution. A short distance and similar substrates/product directionality in the active sites between TsaC and TsaD offer a necessary condition for an effective transfer. An effective proxy for the general binding affinity to both enzymes' active sites can be the number of hydrogen bonds formed

to the adenosine ring. The increased number of hydrogen bonds to the substrate by TsaD as compared to TsaC, combined with a short distance to diffuse a synthesized unstable intermediate, TC-AMP, provides a feasible driving force for a rapid transfer and for the stabilization of TC-AMP.

The structures and the mechanism of TsaC have been extensively investigated. Despite this research effort, the catalytic mechanism remains unclear, and the main question of what is the preferred substrate, CO_2 or HCO_3^- , has not been decisively resolved. After an extensive review of the existing literature, we decided to produce a 3-D model of the binding of substrates to shed light on the steric and electronic requirements imposed by the TsaC active site. The comparison between the details of different structures indicated several important features.

The first is that TsaC structures lack a distinct and specific metal ion binding site that would drive and organize the sequential binding of substrates. Metal ions are detected only in structures with bound nucleotides. This fact can be attributed to the necessity of charge neutralization of nucleotide triphosphates in solution. The presence of metal counterions bound to the nucleotides suggests that upon binding of the nucleotides, the metal ion would be brought to the active site of the particular protein with them. In models of TsaC/C2 structures with bound metal ions such as *T. maritima*, *P. abyssi*, and *S. tokodaii*, the only residue that directly coordinates the metal ion is Ser, which explains its rather weak affinity to the apo-protein.

The second important feature is that there is a well-defined and conserved location for L-Thr, which stands in contrast to variations/shifts in the positions of the phosphates of nucleotides in different structures. The structure containing the L-Thr and the AMPPNP shows a significant shift of the alpha phosphate compared to that containing the product TC-AMP. This feature suggests that binding of L-Thr provides a structural base for binding of the second ligand (CO_2 or CO_3^-), which in turn facilitates binding of the ATP with the associated metal ion. Most likely, the incoming metal ion (Mg^{2+}) binds not only the triphosphate but also the second ligand, CO_2 or CO_3^- .

The lack of a well-defined metal ion binding site clearly projects onto the problem of selecting which of the substrates is preferred by TsaC: CO_2 or CO_3^- . The enzymes utilizing the gaseous CO_2 , such as RUBISCO or carbonic anhydrase (CA), provide restrictive conditions for the binding of this molecule. As the presence of dissolved CO_2 dramatically drops with increased pH, in both enzymes there is a strongly bound metal ion to organize their active sites, and additionally, in vivo, the cells utilize an additional mechanism for concentrating the CO_2 . Both methods must be used by the enzymes, as the natural solubility and availability of CO_2 would limit the catalytic turnover. Clearly, the TsaC enzymes do not have any of these requirements fulfilled. Even in enzymes that were suggested to use CO_2 , such as biotin carboxylase, the use of metal ions and transient CO_3^- intermediates that produce carboxyphosphate [46] suggests that CO_3^- is a much more abundant and dominant species.

Considering all these factors and the relative availability of CO_2 or CO_3^- , it becomes natural to consider the possibility that HCO_3^- is a preferred substrate for the TsaC/C2. Additional experimental support for this choice is provided by the structure of *Pyrococcus abyssi* Sua5 (6F89), in which, for the first time, CO_3^- was tentatively captured [19]. However, despite our clear preference for CO_3^- as a ligand, we need to consider a model for CO_2 initiating the reaction. To provide an equal basis to compare the advantages and drawbacks of the particular scheme we sketched out below, both schemes are shown in Figure 6. Based on all these observations, we proposed the catalytic mechanism for the TsaC-like enzymes (threonylcarbamoylate synthase) and constructed the 3-D model of its initial state and subsequent intermediates (Figure 6) for both alternative mechanisms.

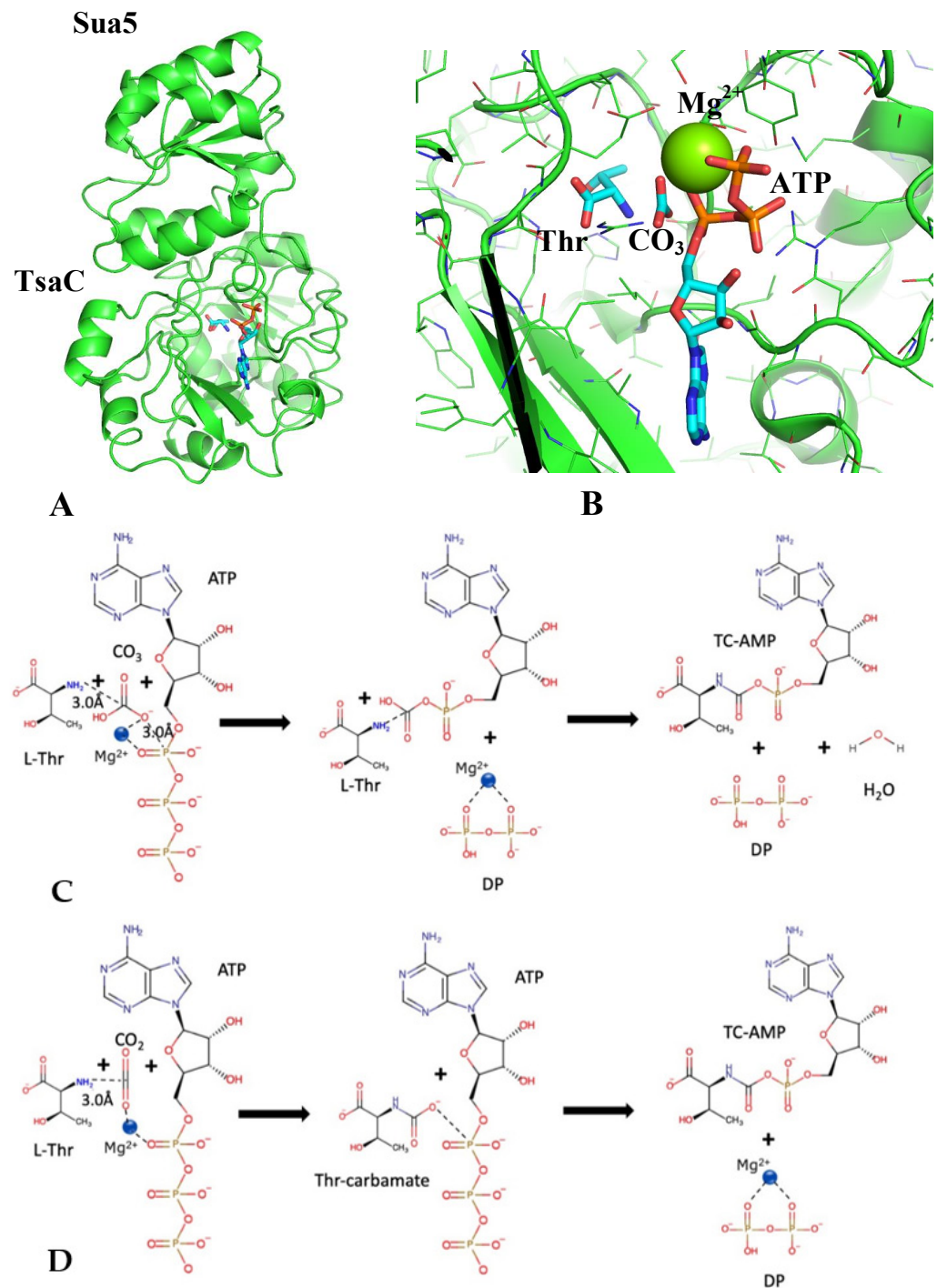


Figure 6. (A) The model of the TsaC2-like subunit (Sua5 from *S. tokodaii*, 3AJE). (B) A close-up of the active site with a model of three bound substrates. The model is derived from 3AJE by conformational change of the phosphate groups of ATP. The L-Thr and the adenosine ring of ATP are at the same locations as in 3AJE, while other elements are placed in chemically and sterically acceptable positions. The carbonate ion is modeled in the position occupied originally by the alpha phosphate of ATP. Further support for such a location comes from the structure (6F89). (C) The schematic of the reaction catalyzed by TsaC. Binding of substrates is sequential: first the L-Thr, then subsequently the CO₃, and finally ATP closing the active site. The reaction is initiated by the nucleophilic attack of the activated CO₃ on the alpha phosphate of ATP. Upon the creation of unstable intermediate carboxy-AMP, the carboxy group is attacked by the activated amino group of the Thr, which forms a transient tetrahedral group. This unstable intermediate collapses and results in the formation of TC-AMP, diphosphate,

and a water molecule. The entire process of binding and chemical transformation is facilitated by the weakly bound Mg^{2+} ion, which most likely serves as a counter ion to the triphosphate and leaves with the diphosphate. (D) The alternative schematic of the reaction catalyzed by TsaC. Binding of substrates is sequential, as above: first the L-Thr, then subsequently the carbon dioxide CO_2 , finally ATP. The reaction is initiated by the nucleophilic attack of the activated amine of the Thr on the carbon of CO_2 . Upon creation of a stable carbamate on the Thr, the newly formed carbamate group attacks the ATP. The second reaction is primed and facilitated by the transiently bound Mg^{2+} . This attack results in the formation of TC-AMP with a diphosphate as a leaving group. The weakly bound Mg^{2+} ion that acts serves as an activator, and the counter ion to the triphosphate leaves with the diphosphate, thus releasing a short-lived TC-AMP.

The proposal for the mechanism was aided by the 3-D model of the substrates bound to TsaC2. The model of the TsaC2 with all three substrates at the active site was obtained in the following manner. The model was generated from the model of TsaC2 with ATP and Thr (3AJE). This model was compared/superposed with the model of the TsaC2 with the product of the reaction TC-AMP (4E1B). This comparison revealed the conformational/rotational change/movement of the alpha phosphate of the ATP. Modeling this motion created room for the third substrate, CO_3 , sandwiched between the Thr and the alpha phosphate of the ATP. In placing the CO_3 , we were guided by the model (6Z81). The final model was created by adjusting the initial locations of CO_3 and ATP for optimal contacts and postulating the location of the metal in the active site. The resulting model is shown in Figure 6B and in Figure S7.

Both mechanisms require the sequential binding of the substrates: first, L-Thr; second, CO_2 or CO_3 ; and last, adenosine triphosphate (ATP). In our preferred mechanism, where the substrate is CO_3 , the reaction must proceed through the condensation of three sequentially bound substrates: L-threonine, CO_3 , and ATP (Figure 6B) and would produce (TC-AMP), diphosphate, and a water molecule. For details of the reaction, please refer to the schematic presented in Figure 6C. In the first step, the activated/deprotonated form of carbonate performs a nucleophilic attack with the O^- group on the alpha phosphate of adenosine, and by inversion of configuration, it produces carboxy-AMP and diphosphate as a leaving group. This happens as soon as the adenosine triphosphate binds and brings the metal ion to the active site, where it coordinates the carbonate ion and the phosphate group of ATP. Incidentally, highly unstable carboxy-AMP was tentatively captured in structure 6N9A [11]. Carboxy-AMP is unstable because it is prone to a nucleophilic attack by the water molecule, so in an aqueous environment, it would undergo excision of the carboxyl group in reaction with the water molecule, thus re-creating carbonate. In the active site of the enzyme, in the absence of an activated water molecule, the deprotonated amine group (NH_2) of Thr performs the nucleophilic attack, and the collapsing tetrahedral intermediate produces the product threonylcarbamoylate-AMP (TC-AMP) with the release of a water molecule. This step is very reminiscent of a standard Schiff base mechanism in which a proton is transferred from the amine group to the leaving oxygen, thus releasing a water molecule. The unstable product TC-AMP is subsequently transferred to the active site of TsaD, which performs the final step of the t^6A_{37} pathway, as described before.

If one assumes that the preferred ligand is CO_2 , then the only choice for the initial step would be a nucleophilic attack of the amine group of Thr to create the carbamyl group at the terminal nitrogen. In a subsequent step, this carbamate would have to attack the alpha phosphate of ATP to produce the threonylcarbamoylate-AMP (TC-AMP) with a concomitant release of a diphosphate.

Both choices for the reaction have ample support in the literature. However, our modeling of the 3-D structures strongly supports the view that a preferred ligand is CO_3 . There is no apparent chemical signature for CO_2 binding to the TsaC/C2 active site; therefore, there is no apparent activation mechanism for CO_2 activation to complete the carbamate formation. Additionally, CO_2 abundance at pH ~ 7.5 , which is routinely utilized in kinetic experiments and probably prevails at physiological conditions, would indicate that its

concentration is below 1%, as judged by the Bjerrum plot. Hence the dominant form would be CO₃ at this pH value, with a 99:1 ratio. Finally, there are many examples of CO₃ interactions with phosphates and the production of unstable intermediates. The best examples are provided by the structures and biochemistry of carbamoyl-phosphate synthase [46,47]. Nevertheless, to resolve the problem of preferred ligands, careful biochemical experiments mapping the entire pH profile for such a reaction should be performed.

4. Summary

In this report, we focused on understanding the last step of the t⁶A₃₇ tRNA modification pathway, i.e., binding of the tRNA to the TsaD-like protein. This inquiry included a review of all available structural information available to date and led to a proposal for the main steps in the entire pathway. These steps are the catalytic mechanism for TsaC/C2 and TsaD, which included the TC-AMP biosynthesis, transfer to TsaD and binding in its active site, and finally the transfer of the TC group to the adenosine 37 of tRNA. We initially focused on proposing a consensus pose of the tRNA molecule binding to the common evolutionary conserved subunit TsaD-like proteins. This process was made possible by reviewing all relevant models and completing them, specifically the models of TsaBDE complex-6FPE, *T. maritima*, and Qri7-3WUH from yeast.

The corrections to the model of Qri7 were less extensive and were carried out to obtain the proper electrostatic image of the protein necessary for docking experiments. In contrast, the corrections to the TsaBDE model 6FPE and finally to 6S84 were more consequential. As elucidated in the Supplement and in [29], the original model 6FPE has been improved to match the quality of the higher resolution model 6N9A [11]. The improved model was shared with the authors of the original model 6FPE, which precipitated the publication of a higher resolution model 6S84 as the Corrigendum [2]. Further evaluation of the data and the model showed that the data for 6S84 were weaker than those for 6FPE, and the quality of the 6S84 model was lower than that of our final model, 6NAK, which contained TC-AMP at the active site. More details of this process have been provided in the epilogue of the Supplement.

The structural improvements played a key role in understanding the tRNA binding modes and established a rational basis for further experimentation. Docking experiments with the homologous TsaD-like component of the pathway from different kingdoms of life resulted in the discovery of the universal mode of binding of tRNA to TsaD. The highly similar positioning of the tRNA against the TsaD suggested by this study attests to the evolutionary relationships between TsaD subunits of different complexes and also highlights the common mechanism of catalysis by TsaD-like and TsaC-like components and their mutual communication. The presence of TsaD in a variety of protein arrangements shows how diverse control mechanisms emerged in different systems. All the findings presented here are in full agreement with previously described biochemical results [4,11] and provide a constructive platform for molecular understanding of this entire pathway. Additionally, the hypothesis presented in this report provides a useful basis for experimental confirmation of the tRNA binding mode and the catalytic mechanisms by biochemical experimentation.

Supplementary Materials: The following supporting information can be downloaded at: <https://www.mdpi.com/article/10.3390/biophysica3020019/s1>, Figure S1: The general view of the final refined B2D2E2 complex (6NAK) in C-alpha representation; Figure S2: The electron density and model improvements during the refinement; Figure S3: The electron density at 0.9 sigma level and model improvements in the region of 30–50 of the TsaD subunit; Figure S4: Comparison of the refined models of the ligand found at the active site of subunit TsaD; Figure S5: Comparison of the refined models of the C-terminal helix of subunit TsaE; Figure S6: The stereo representation of the active site of TsaD containing refined TC-AMP with docked tRNA; Figure S7: The stereo representation of the active site of TsaC2, containing refined Thr (3AJE), conformationally adjusted ATP, and manually modeled CO₃ and Mg²⁺; Table S1: Refinement statistics of the original and refined model of *T. maritima* TsaB-TsaD-TsaE complex in B2D2E2 composition and Qri7 from yeast.

Funding: This research received no external funding.

Data Availability Statement: The corrected structures of TsaBDE complex as well as Qri7 were deposited in PDB under codes 6NAK and 6NBJ.

Acknowledgments: The author wanted to thank Daniel Stec for his careful reading of the manuscript and useful remarks.

Conflicts of Interest: The author declares no conflict of interest.

References

1. Su, C.; Jin, M.; Zhang, W. Conservation and Diversification of tRNA^{t6A}-Modifying Enzymes across the Three Domains of Life. *Int. J. Mol. Sci.* **2022**, *23*, 13600. [[CrossRef](#)] [[PubMed](#)]
2. Missouri, S.; Plancqueel, S.; Li de la Sierra-Gallay, I.; Zhang, W.; Liger, D.; Durand, D.; Dammak, R.; Collinet, B.; van Tilbeurgh, H. The structure of the TsaB/TsaD/TsaE complex reveals an unexpected mechanism for the bacterial t6A tRNA-modification. *Nucleic Acids Res.* **2018**, *46*, 5850–5860, Corrigendum in *Nucleic Acids Res.* **2019**, *47*, 9464–9465. [[CrossRef](#)]
3. Deutsch, C.; El Yacoubi, B.; de Crécy-Lagard, V.; Iwata-Reuyl, D. Biosynthesis of Threonylcarbamoyl Adenosine (t6A), a Universal tRNA Nucleoside. *J. Biol. Chem.* **2012**, *287*, 13666–13673. [[CrossRef](#)] [[PubMed](#)]
4. Luthra, A.; Swinehart, W.; Bayooz, S.; Phan, P.; Stec, B.; Iwata-Reuyl, D.; Swairjo, M.A. Structure and mechanism of a bacterial t6A biosynthesis system. *Nucleic Acids Res.* **2018**, *46*, 1395–1411. [[CrossRef](#)] [[PubMed](#)]
5. Perrochia, L.; Guetta, D.; Hecker, A.; Forterre, P.; Basta, T. In vitro biosynthesis of a universal t6A tRNA modification in Archaea and Eukarya. *Nucleic Acids Res.* **2013**, *41*, 9484–9499. [[CrossRef](#)] [[PubMed](#)]
6. Lauhon, C.T. Mechanism of N6-threonylcarbamoyladenonsine (t6a) biosynthesis: Isolation and characterization of the intermediate threonylcarbamoyl-AMP. *Biochemistry* **2012**, *51*, 8950–8963. [[CrossRef](#)]
7. El Yacoubi, B.; Lyons, B.; Cruz, Y.; Reddy, R.; Nordin, B.; Agnelli, F.; Williamson, J.R.; Schimmel, P.; Swairjo, M.A.; de Crécy-Lagard, V. The universal YrdC/Sua5 family is required for the formation of threonylcarbamoyladenonsine in tRNA. *Nucleic Acids Res.* **2009**, *37*, 2894–2909. [[CrossRef](#)]
8. Torrent, M.; Chalancon, G.; de Groot, N.S.; Wuster, A.; Babu, M.M. Cells alter their tRNA abundance to selectively regulate protein synthesis during stress conditions. *Sci. Signal.* **2018**, *11*, eaat6409. [[CrossRef](#)]
9. Parthier, C.; Gorlich, S.; Jaenecke, F.; Breithaupt, C.; Brauer, U.; Fandrich, U.; Clausnitzer, D.; Wehmeier, U.F.; Bottcher, C.; Scheel, D.; et al. The O-Carbamoyltransferase TobZ catalyzes an ancient enzymatic reaction. *Angew. Chem. Int. Ed. Engl.* **2012**, *51*, 4046–4052. [[CrossRef](#)]
10. Petkun, S.; Shi, R.; Li, Y.; Asinas, A.; Munger, C.; Zhang, L.; Waclawek, M.; Soboh, B.; Sawers, R.G.; Cygler, M. Structure of hydrogenase maturation protein HypF with reaction intermediates shows two active sites. *Structure* **2011**, *19*, 1773–1783. [[CrossRef](#)]
11. Luthra, A.; Paranagama, N.; Swinehart, W.; Bayooz, S.; Phan, P.; Quach, V.; Schiffer, J.M.; Stec, B.; Iwata-Reuyl, D.; Swairjo, M.A. Conformational communication mediates the reset step in t6A biosynthesis. *Nucleic Acids Res.* **2019**, *47*, 6551–6567. [[CrossRef](#)] [[PubMed](#)]
12. Srinivasan, M.; Mehta, P.; Yu, Y.; Prugar, E.; Koonin, E.V.; Karzai, A.W.; Sternglanz, R. The highly conserved KEOPS/EKC complex is essential for a universal tRNA modification, t6A. *EMBO J.* **2010**, *30*, 873–881. [[CrossRef](#)] [[PubMed](#)]
13. Zhang, W.; Collinet, B.; Graille, M.; Daugeron, M.-C.; Lazar, N.; Libri, D.; Durand, D.; van Tilbeurgh, H. Crystal structures of the Gon7/Pcc1 and Bud32/Cgi121 complexes provide a model for the complete yeast KEOPS complex. *Nucleic Acids Res.* **2015**, *43*, 3358–3372. [[CrossRef](#)] [[PubMed](#)]
14. Thiaville, P.C.; Iwata-Reuyl, D.; de Crécy-Lagard, V. Diversity of the biosynthesis pathway for threonylcarbamoyladenonsine (t(6)A), a universal modification of tRNA. *RNA Biol.* **2014**, *11*, 1529–1539. [[CrossRef](#)]
15. Vagin, A.A.; Steiner, R.A.; Lebedev, A.A.; Potterton, L.; McNicholas, S.; Long, F.; Murshudov, G.N. REFMAC5 dictionary: Organization of prior chemical knowledge and guidelines for its use. *Acta Crystallogr. Biol. Crystallogr.* **2004**, *60*, 2184–2195. [[CrossRef](#)] [[PubMed](#)]
16. Tominaga, T.; Kobayashi, K.; Ishii, R.; Ishitani, R.; Nureki, O. Structure of *Saccharomyces cerevisiae* mitochondrial Qri7 in complex with AMP. *Acta Crystallogr. Sect. F* **2014**, *70*, 1009–1014. [[CrossRef](#)] [[PubMed](#)]
17. Mao, D.Y.L.; Neculai, D.; Downey, M.; Orlicky, S.; Haffani, Y.Z.; Ceccarelli, D.F.; Ho, J.S.L.; Szilard, R.K.; Zhang, W.; Ho, C.S.; et al. Atomic structure of the KEOPS complex: An ancient protein kinase-containing molecular machine. *Mol. Cell* **2008**, *32*, 259–275. [[CrossRef](#)]
18. Sankaranarayanan, R.; Dock-Bregeon, A.C.; Romby, P.; Caillet, J.; Springer, M.; Rees, B.; Ehresmann, C.; Ehresmann, B.; Moras, D. The Structure of Threonyl-tRNA Synthetase-tRNAThr Complex Enlightens Its Repressor Activity and Reveals an Essential Zinc Ion in the Active Site. *Cell* **1999**, *97*, 371–381. [[CrossRef](#)]
19. Pichard-Kostuch, A.; Zhang, W.; Liger, D.; Daugeron, M.-C.; Létoquart, J.; de la Sierra-Gallay, I.L.; Forterre, P.; Collinet, B.; van Tilbeurgh, H.; Basta, T. Structure–function analysis of Sua5 protein reveals novel functional motifs required for the biosynthesis of the universal t6A tRNA modification. *RNA* **2018**, *24*, 926–938. [[CrossRef](#)]

20. Agari, Y.; Sato, S.; Wakamatsu, T.; Bessho, Y.; Ebihara, A.; Yokoyama, S.; Kuramitsu, S.; Shinkai, A. X-ray crystal structure of a hypothetical Sua5 protein from *Sulfolobus tokodaii* strain 7. *Proteins* **2008**, *70*, 1108–1111. [[CrossRef](#)]
21. Kuratani, M.; Kasai, T.; Akasaka, R.; Higashijima, K.; Terada, T.; Kigawa, T.; Shinkai, A.; Bessho, Y.; Yokoyama, S. Crystal structure of *Sulfolobus tokodaii* Sua5 complexed with L-threonine and AMPPNP. *Proteins Struct. Funct. Bioinform.* **2011**, *79*, 2065–2075. [[CrossRef](#)] [[PubMed](#)]
22. Teplova, M.; Tereshko, V.; Sanishvili, R.; Joachimiak, A.; Bushueva, T.; Anderson, W.F.; Egli, M. The structure of the yrdC gene product from *Escherichia coli* reveals a new fold and suggests a role in RNA binding. *Protein Sci.* **2000**, *9*, 2557–2566. [[CrossRef](#)] [[PubMed](#)]
23. Kopina, B.J.; Missouri, S.; Collinet, B.; Fulton, M.G.; Cirio, C.; van Tilbeurgh, H.; Lauhon, C.T. Structure of a reaction intermediate mimic in t6A biosynthesis bound in the active site of the TsaBD heterodimer from *Escherichia coli*. *Nucleic Acids Res.* **2021**, *49*, 2141–2160. [[CrossRef](#)] [[PubMed](#)]
24. Zhang, W.; Collinet, B.; Perrochia, L.; Durand, D.; van Tilbeurgh, H. The ATP-mediated formation of the YgjD–YeaZ–YjeE complex is required for the biosynthesis of tRNA t6A in *Escherichia coli*. *Nucleic Acids Res.* **2015**, *43*, 1804–1817. [[CrossRef](#)] [[PubMed](#)]
25. Nichols, C.E.; Lamb, H.K.; Thompson, P.; El Omari, K.; Lockyer, M.; Charles, I.; Hawkins, A.R.; Stammers, D.K. Crystal structure of the dimer of two essential *Salmonella typhimurium* proteins, YgjD & YeaZ and calorimetric evidence for the formation of a ternary YgjD–YeaZ–YjeE complex. *Protein Sci.* **2013**, *22*, 628–640. [[PubMed](#)]
26. Hecker, A.; Lopreiato, R.; Graille, M.; Collinet, B.; Forterre, P.; Libri, D.; van Tilbeurgh, H. Structure of the archaeal Kae1/Bud32 fusion protein MJ1130: A model for the eukaryotic EKC/KEOPS subcomplex. *EMBO J.* **2008**, *27*, 2340–2351. [[CrossRef](#)]
27. Painter, J.; Merritt, E.A. Optimal description of a protein structure in terms of multiple groups undergoing TLS motion. *Acta Crystallogr. Sect. D Biol. Crystallogr.* **2006**, *62*, 439–450. [[CrossRef](#)]
28. Stec, B.; Zhou, R.; Teeter, M.M. Full-matrix refinement of the protein crambin at 0.83 Å and 130 K. *Acta Crystallogr. Sect. D Biol. Crystallogr.* **1995**, *51*, 663–681. [[CrossRef](#)]
29. Stec, B. Comments on the recent crystal structure of TsaBDE complex of bacterial t6A biosynthesis system and its significance for understanding TC-AMP processing. *bioRxiv* **2019**. [[CrossRef](#)]
30. Schrödinger, L.; DeLano, W. PyMOL. 2020. Available online: <http://www.pymol.org/pymol> (accessed on 15 October 2015).
31. van Zundert, G.C.P.; Rodrigues, J.P.G.L.M.; Trellet, M.; Schmitz, C.; Kastiris, P.L.; Karaca, E.; Melquiond, A.S.J.; van Dijk, M.; de Vries, S.J.; Bonvin, A.M.J.J. The HADDOCK2.2 web server: User-friendly integrative modeling of biomolecular complexes. *J. Mol. Biol.* **2016**, *428*, 720–725. [[CrossRef](#)]
32. Morris, G.M.; Huey, R.; Lindstrom, W.; Sanner, M.F.; Belew, R.K.; Goodsell, D.S.; Olson, A.J. AutoDock4 and AutoDock-Tools4: Automated docking with selective receptor flexibility. *J. Comput. Chem.* **2009**, *30*, 2785–2791. [[CrossRef](#)] [[PubMed](#)]
33. Tuszyńska, I.; Magnus, M.; Jonak, K.; Dawson, W.; Bujnicki, J.M. NPdock: A web server for protein–Nucleic acid docking. *Nucleic Acids Res.* **2015**, *43*, W425–W430. [[CrossRef](#)] [[PubMed](#)]
34. Xu, Q.; McMullan, D.; Jaroszewski, L.; Krishna, S.S.; Elsliger, M.-A.; Yeh, A.P.; Abdubek, P.; Astakhova, T.; Axelrod, H.L.; Carlton, D.; et al. Structure of an essential bacterial protein YeaZ (TM0874) from *Thermotoga maritima* at 2.5 Å resolution. *Acta Crystallogr. Sect. F* **2010**, *66*, 1230–1236. [[CrossRef](#)] [[PubMed](#)]
35. Teplyakov, A.; Obmolova, G.; Tordova, M.; Thanki, N.; Bonander, N.; Eisenstein, E.; Howard, A.J.; Gilliland, G.L. Crystal structure of the YjeE protein from *Haemophilus influenzae*: A putative Atpase involved in cell wall synthesis. *Proteins Struct. Funct. Bioinform.* **2002**, *48*, 220–226. [[CrossRef](#)] [[PubMed](#)]
36. Wan, L.C.K.; Mao, D.Y.L.; Neculai, D.; Strecker, J.; Chiovitti, D.; Kurinov, I.; Poda, G.; Thevakumaran, N.; Yuan, F.; Szilard, R.K.; et al. Reconstitution and characterization of eukaryotic N6-threonylcarbamoylation of tRNA using a minimal enzyme system. *Nucleic Acids Res.* **2013**, *41*, 6332–6346. [[CrossRef](#)]
37. Liu, Y.-Y.; He, M.-H.; Liu, J.-C.; Lu, Y.-S.; Peng, J.; Zhou, J.-Q. Yeast KEOPS complex regulates telomere length independently of its t6A modification function. *J. Genet. Genom.* **2018**, *45*, 247–257. [[CrossRef](#)]
38. Beenstock, J.; Ona, S.M.; Porat, J.; Orlicky, S.; Wan, L.C.K.; Ceccarelli, D.F.; Maisonneuve, P.; Szilard, R.K.; Yin, Z.; Setiapatra, D.; et al. A substrate binding model for the KEOPS tRNA modifying complex. *Nat. Commun.* **2020**, *11*, 6233. [[CrossRef](#)]
39. Beenstock, J.; Sicheri, F. The structural and functional workings of KEOPS. *Nucleic Acids Res.* **2021**, *49*, 10818–10834. [[CrossRef](#)]
40. Wang, J.T.; Zhou, J.B.; Mao, X.L.; Zhou, L.; Chen, M.; Zhang, W.; Wang, E.D.; Zhou, X.L. Commonality and diversity in tRNA substrate recognition in t6A biogenesis by eukaryotic KEOPSs. *Nucleic Acids Res.* **2022**, *50*, 2223–2239. [[CrossRef](#)]
41. Watson, J.D.; Crick, F.H.C. Genetical implications of the structure of deoxyribonucleic acid. *Nature* **1953**, *171*, 964–967. [[CrossRef](#)]
42. Singh, V.; Fedeles, B.I.; Essigmann, J.M. Role of tautomerism in RNA biochemistry. *RNA* **2014**, *21*, 1–13. [[CrossRef](#)] [[PubMed](#)]
43. Verma, N.; Groshong, A.; Caimano, M.J.; Hawley, K.L.; Luthra, A. Structural Modeling of t6A Biosynthesis System and Flexibility Analysis of TsaC2 in *Borrelia*. In *Proceedings of the North Eastern Structure Symposium 2020 Structural Biology of Host-Pathogen Interactions, 24 October 2020*; University of Connecticut: Storrs, CT, USA, 2020.
44. Wang, Q.; Xia, J.; Guallar, V.; Krilov, G.; Kantrowitz, E.R. Mechanism of thermal decomposition of carbamoyl phosphate and its stabilization by aspartate and ornithine transcarbamoylases. *Proc. Natl. Acad. Sci. USA* **2008**, *105*, 16918–16923. [[CrossRef](#)] [[PubMed](#)]
45. Chou, C.-Y.; Yu, L.P.C.; Tong, L. Crystal Structure of Biotin Carboxylase in Complex with Substrates and Implications for Its Catalytic Mechanism. *J. Biol. Chem.* **2009**, *284*, 11690–11697. [[CrossRef](#)] [[PubMed](#)]

46. Huang, X.; Holden, H.M.; Raushel, F.M. Channeling of Substrates and Intermediates in Enzyme-Catalyzed Reactions. *Annu. Rev. Biochem.* **2001**, *70*, 149–180. [[CrossRef](#)] [[PubMed](#)]
47. Powers, S.; Meister, A. Carbonic-phosphoric anhydride (carboxy phosphate). Significance in catalysis and regulation of glutamine-dependent carbamyl phosphate synthetase. *J. Biol. Chem.* **1978**, *253*, 1258–1265. [[CrossRef](#)] [[PubMed](#)]

Disclaimer/Publisher’s Note: The statements, opinions and data contained in all publications are solely those of the individual author(s) and contributor(s) and not of MDPI and/or the editor(s). MDPI and/or the editor(s) disclaim responsibility for any injury to people or property resulting from any ideas, methods, instructions or products referred to in the content.